International Journal of Bioprinting

RESEARCH ARTICLE

Combination of 3D printing and electrospinning to develop chitin/gelatin/PVA scaffolds

Teresa Carranza[1], Jone Uranga[1], Ainhoa Irastorza[2], Ander Izeta[2], Pedro Guerrero[1,3,4]*, Koro de la Caba[1,3]*

[1]BIOMAT Research Group, University of the Basque Country (UPV/EHU), Escuela de Ingeniería de Gipuzkoa, Plaza de Europa 1, 20018 Donostia-San Sebastián, Spain

[2]Biodonostia Health Research Institute, Tissue Engineering Group, P° Dr. Beguiristain s/n, 20014, Donostia-San Sebastián, Spain

[3]BCMaterials, Basque Center for Materials, Applications and Nanostructures, UPV/EHU Science Park, 48940, Leioa, Spain

[4]Proteinmat materials SL, Avenida de Tolosa 72, 20018 Donostia-San Sebastián, Spain

(This article belongs to the *Special Issue: Advances in the Application of Bioprinted Biomaterials in Tissue Engineering*.)

Abstract

In this study, novel scaffolds based on natural polymers were developed by combining 3D printing (3DP) and electrospinning (ES) techniques. ES ink was prepared with gelatin and poly(vinyl alcohol) (PVA), while 3DP ink was prepared with gelatin and chitin. Different biopolymers were used to confer unique properties to each ink and obtain a multilayered scaffold suitable for tissue regeneration. First, gelatin is able to exhibit the characteristics needed for both inks since gelatin chains contain arginine-glycine-aspartic (RGD) motifs, an important sequence in the promotion of cell adhesion, which gives gelatin an improved biological behavior in comparison to other polymers. Additionally, PVA was selected for ES ink to facilitate gelatin spinnability, and chitin was incorporated into 3DP ink as reinforcement to provide mechanical support and protection to the overall design. In this work, chitin was extracted from fruit fly pupae. The high extraction yield and purity of the chitin obtained from the fruit fly pupae confirmed that this pupa is an alternative source to produce chitin. Once the chitin was characterized, both inks were prepared and rheological analysis was carried out in order to confirm the shear thinning behavior required for additive manufacturing processes. The combination of 3DP and ES processes resulted in porous scaffolds, which were proven biocompatible, highlighting their potential for biomedical applications.

Keywords: Fruit fly pupae; Chitin; Gelatin; 3D printing; Electrospinning; Scaffolds

***Corresponding authors:**
Pedro Guerrero
(pedromanuel.guerrero@ehu.es)

Koro de la Caba
(koro.delacaba@ehu.es)

Citation: Carranza T, Uranga J, Irastorza A, *et al*., 2023, Combination of 3D printing and electrospinning to develop chitin/gelatin/PVA scaffolds. *Int J Bioprint,* 9(3): 701.
https://doi.org/10.18063/ijb.701

Received: October 04, 2022
Accepted: November 05, 2022
Published Online: March 6, 2023

1. Introduction

Millions of tonnes of biowaste are generated annually by agricultural and industrial activities[1], leading to a diverse array of environmental issues[2,3]. The potential of biowaste to produce value-added products can help boost the circular economy and lead to a significant reduction in the amounts of waste generated and to the efficiency in the use of resources. In this context, fruit fly pupae (*Ceratitis capitata*) can be

assessed as an alternative source for chitin extraction. *C. capitata* causes indirect economic losses in fruit production and thus, different strategies are employed for an integrated pest management of fruit flies, such as the sterile insect technology, in which large quantities of pupae are generated[4]. These pupae represent a source of chitin, since this polysaccharide with unique technological properties is the major organic component in pupae (around 86% of the total weight)[5]. Chitin is the second most abundant polysaccharide in nature and it has a long history of scientific studies, such as those for biomedical applications[6]. Moreover, chitin can be employed to enhance the functional properties of other biopolymers, such as gelatin, which can also be extracted from biowastes[7,8].

Several technologies have been employed to obtain products from available, zero-cost, and biodegradable wastes[9]; among them, 3D printing (3DP) and electrospinning (ES) have been utilized[10]. On the one hand, 3DP techniques are known since 1986, when Charles Hull introduced 3D lithography technology[11]. This technology never cease to develop and provide solutions in different sectors, such as automotive, aerospace, dental, and biomedical fields; sometimes, it is used to obtain prototypes and final parts[12-14]. Nowadays, 3DP techniques are gaining interest because of their unique capacity to deposit biological and non-biological components to mimic the extracellular matrix and provide the required microenvironment to ensure cell adhesion, migration, and replication[15,16]. In this regard, adding chitin to gelatin-based inks can lead to the formulation of inks with enhanced properties, such as good adhesion performance, biological compatibility, and appropriate biodegradability rate[17], with potential for wound healing applications[18]. On the other hand, ES is a technique to obtain nano- and/or micro-fibers with high area/volume ratio via an electric field[19,20]. High voltage and constant feed rate are applied to a polymer solution, making the electrostatic repulsion force overcome surface tension, and ejecting the polymer solution to the ground. In this process, the solvent is evaporated and the polymer is deposited to form a porous mat. In this regard, poly(vinyl alcohol) (PVA) is frequently blended with other polymers, such as gelatin or sodium alginate, in order to ensure the spinnability of natural polymers due to its water solubility, biocompatibility, and biodegradability[19].

Taking the above into consideration, chitin/gelatin/PVA scaffolds were prepared in this work for biomedical applications. Since scaffolds should replicate the morphology and the function of target tissue[21,22], morphology requirements are related to the scaffold porosity, a limiting factor to ensure new tissue formation[23]. Both macro- and micro-porosity, as well as interconnectivity between pores, are required[23,24]. To address all these challenges, the combination of 3DP and ES is carried out in this work, using both techniques in a sequential mode to get a sandwich-type hybrid structure. Although some works have been carried out with chitosan and gelatin inks[25,26], the incorporation of chitin into gelatin-based ink is a novel approach to improve cellular adhesion and protect cells from bacterial colonization. In this work, a complete assessment was carried out, from the optimization of the chitin extraction to the characterization of the final scaffolds to evaluate their viability for biomedical applications.

2. Materials and methods

2.1. Materials

Porcine gelatin (250 bloom) was supplied by Sancho de Borja SL (Spain). Chitin was extracted from the fruit fly pupae (*C. capitata*), which were supplied by TRAGSA (Spain). Glycerol (99.01% purity) and acetic acid were obtained from Panreac (Spain), and PVA was provided by Sigma-Aldrich (USA). NaOH and H_2O_2 employed for the chitin extraction were purchased from Panreac (Spain) and Honeywell (Germany), respectively.

2.2. Sample preparation

2.2.1. Extraction of chitin from fruit fly pupae

The chitin extraction procedure followed in this work was selected based on previous experiments in order to optimize the yield and increase the resources efficiency, both environmental and economical. Hence, in this work, 50 g of fruit fly pupae were washed with water to remove impurities and treated with NaOH (1 M) at room temperature for 24 h under continuous stirring. Then, samples were filtered and the solid fraction (chitin) was washed with distilled water up to neutral pH. Prior to use, chitin was decolored with H_2O_2 in a ratio of 1:20 (w/v) at room temperature for 2 h. The mixture was filtered and the solid fraction was dried in an oven at 40°C for 24 h. Finally, chitin was milled to obtain the powder.

2.2.2. 3DP ink preparation

3DP ink was prepared by dissolving 8 wt% gelatin in distilled water together with 5 wt% chitin (based on gelatin mass) and 30 wt% glycerol (based on gelatin mass). The mixture was kept at 85°C under constant stirring for 30 min. Then, the pH was adjusted to 7 with NaOH (1 M) and the sample was stirred at 8000 rpm for 300 s with an IKA S 25N-18G-ST ULTRA-TURRAX homogenizer (IKA-Werke, Germany) using a 18 mm head. Finally, mixtures were poured into 3D printing syringes and stored in a fridge at 4°C until further analysis.

Table 1. Processing conditions used to prepare 3DP-ES scaffolds

Process parameters	3D printing (3DP)	Electrospinning (ES)
Nozzle/needle size	16 G	22 G
Head temperature	32°C	23°C
Platform temperature	21°C	21°C
Speed	10 mm/s	30 mm/s
Infill density	30%	10%
Applied voltage	–	9.5 kV
Flow	155%	12 µL/min
Layer height	0.3 mm	–
Offset distance	–	9 cm

2.2.3. ES ink preparation

ES ink was prepared using 0.5 M acetic acid as a solvent. First, a 10 wt% PVA solution was prepared at 120°C under magnetic stirring. Once PVA dissolved, the solution was cooled to 85°C and 2 wt% gelatin was added. The resulting solution pH was 3.2.

2.2.4. Scaffold processing

Scaffolds were fabricated with a domoBIO 2A bioprinter (Domotek, Gipuzkoa, Spain), equipped with a syringe extruder, an electrospinning extruder, and a refrigerated platform. An electrospinning adapter with a teflon sheet was used as substrate. The whole process was performed by a single bioprinter, capable of integrating both technologies in a single printing platform. First, the digital structure, consisting of a cylinder of 21 mm diameter and 1.2 mm height, was designed employing a computer-aided design (CAD) software (Solid Edge, Siemens, Germany) and Ultimaker Cura 4.13.1 (Ultimaker BV, the Netherlands) as slicer. The processing parameters are shown in Table 1. The electrospinning solution was run for 1 min per line. 3DP-ES scaffolds were composed by four lines of 3DP layers and three interpenetrating ES lines, resulting in a sandwich-like structure. All scaffolds were stored at a chamber under controlled conditions (25°C, 50% relative humidity). All characterization tests were carried out at least in triplicate.

2.3. Characterization

2.3.1. Chitin extraction yield

First, pupae were weighed (w_p) and, after the extraction process, dry chitin was weighed (w_c). The extraction yield was calculated as shown in Equation I.

$$Extraction\ yield(\%) = \frac{w_c}{w_p} \bullet 100 \quad (I)$$

2.3.2. Fourier transform infrared spectroscopy

Fourier transform infrared (FTIR) analysis was performed using a platinum-ATR Alpha II FTIR spectrometer (Bruker). The chitin spectra were obtained from 800 to 4000 cm^{-1} with a resolution of 4 cm^{-1}.

2.3.3. Differential scanning calorimetry

Differential scanning calorimetry (DSC) was performed using a DSC 822 (Mettler Toledo S.A.E.). About 3.0 ± 0.2 mg of sample were weighed and sealed in aluminum pans, which were heated from 25°C to 250°C at 10°C/min under nitrogen atmosphere (10 mL N_2/min).

2.3.4. Thermo-gravimetric analysis

Thermo-gravimetric analysis (TGA) measurements were carried out using a TGA SDTA 851 (Mettler Toledo S.A.E.). Samples were heated from 25°C to 800°C at 10°C/min under nitrogen atmosphere (10 mL N_2/min).

2.3.5. X-ray diffraction

X-ray diffraction (XRD) analysis was carried out using a diffraction unit (PANalyticXpert PRO). The radiation was generated from a Cu-Kα (λ = 1.5418 Å) source at 40 kV and 40 mA. Data were collected from 2º to 50º, and crystallinity (CrI) was calculated according to the Equation II[27]:

$$CrI = \frac{I_{110} - I_{am}}{I_{110}} \bullet 100 \quad II$$

where I_{110} is the maximum intensity at 20° and I_{am} is the maximum intensity at 13°.

2.3.6. ^{13}C Nuclear magnetic resonance

^{13}C Nuclear magnetic resonance (^{13}C NMR) was performed at 90°C in a Bruker Avance unit, equipped with BBO z-gradient probe, using agar solution at 5% (w/v) in D_2O. About 14,000 scans at 125.75 MHz, spectral window of 25,000 Hz, and recovery delay of 2 s were employed.

2.3.7. Elemental analysis

Elemental analysis (EA) was performed using an Euro EA Elemental Analyser. Carbon (C) and nitrogen (N) contents were used to determine the average degree of acetylation (DA) of chitin, as represented in Equation III[28]:

$$DA = \frac{\left(\frac{C}{N}\right) - 5.14}{1.72} \bullet 100 \quad III$$

where C/N is the carbon/nitrogen ratio.

2.3.8. Rheological analysis

The rheological measurements of inks were performed using Thermo Scientific Haake Rheostress1 Rheometer (IFI S.L., Vigo, Spain), equipped with a 35 mm diameter serrated plate–plate geometry. The gap between plates used was 1 mm for all tests. Experiments were performed keeping the temperature constant at 30°C, 32°C, and 35°C for 3DP ink and 25°C for ES ink.

Strain sweeps were carried out between 0.01% and 100% strain at 1 Hz to determine the linear viscoelastic range (LVR) and the critical strain. Then, frequency sweeps were performed between 0.01 and 50 Hz within the LVR to obtain elastic modulus (G') and viscous modulus (G''). Finally, the shear flow test was carried out from 0.1 to 50 s^{-1}.

Shear sweep data were fitted to cross model for shear thinning fluids[29], represented in Equation IV:

$$\eta = \eta_{\infty} + \frac{\eta_0 - \eta_{\infty}}{1 + (C\dot{\gamma})^m} \quad \text{(IV)}$$

where C is consistency or cross time constant, $\dot{\gamma}$ shear rate, η viscosity, η_0, and η_{∞} viscosity at low and high shear values (zero and infinite shear values), and m dimensionless cross rate constant, calculated by curve fitting in the slope region.

2.3.9. Mucoadhesion test

Mucoadhesion test was carried out using a TA.XT.Plus C Texture Analyzer (Aname, Madrid, Spain) with a 5 kg load cell. Data were collected using 0.1 mm/s test speed, 30 s contact time, 3.2 g trigger force, and 20.4 g applied force. The biological substrate used was a filter paper moistened during 3 min with 1% type II mucin from porcine stomach (Sigma-Aldrich, Madrid, Spain).

2.3.10. Texture profile analysis

A TA.XT.Plus C Texture Analyzer (Aname, Madrid, Spain) with a 5 kg load cell was used to obtain texture profile analysis (TPA). Data were collected at 1 mm/s speed, 20% strain, and 5 g trigger force.

2.3.11. Optical microscopy

Surface characterization was carried out using Nikon Eclipse E600 optical microscope with digital camera (Izasa Scientific,) equipped with 10× objective and 10× eyepieces. Images were analyzed with Image J software[30].

2.3.12. Biocompatibility assessment

The biocompatibility assessment was performed in compliance with the requirements of ISO 10993-5[31]. Human fibroblast HS27 (ECACC) cell line was used for the biocompatibility determination. Following the manufacturer recommendations, fibroblasts were cultured on Dulbecco's Modified Eagle's Medium (DMEM) (Sigma), supplemented with 10% (v/v) inactive fetal bovine serum (FBS) (Lonza), 1% (v/v) penicillin-streptomycin (Lonza), and 1% (v/v) L-glutamine (Sigma) at 37°C in a humidified incubator with a 5% CO_2 atmosphere. Cell passages were performed weekly until confluence. At that point, cells were collected by 0.25% trypsin-EDTA (Sigma) and centrifuged at 1500 rpm for 5 min at room temperature. The obtained pellet was resuspended in the above-mentioned medium to obtain a homogeneous cell suspension, after which 96-well and 24-well plates were seeded with a density of 25,000 cells/cm^2 with 100 and 500 µL of medium, respectively.

After 24 h of seeding, samples were placed in contact with the cells by putting them on top of the cells. Additionally, some wells were left without biomaterial to be included as positive and negative controls. For that, the samples had been previously cut in 5 mm and 8 mm diameter discs for 96-well and 24-well plates, respectively, washed by dialysis in Dulbecco's PBS (DPBS) (Gibco) for 72 h, and sterilized by immersion into 70% ethanol for 5 min and exposing to UV for 15 min. Finally, samples were washed three times for 5 min with DPBS in sterile conditions before placing them into the wells.

Short-term biocompatibility was evaluated in 96-well plates at 24, 48, and 72 h of cell culture after the exposure of the scaffolds. Cell activity was measured based on the reductive capacity of the cells using the colorimetric assay Cell Counting Kit-8 (Sigma). Following the manufacturer's recommendations, the wells were first washed with DPBS and then, the compound was added to the wells at a final concentration of 1:10 in cell medium. After 2 h of incubation at 37°C, the absorbance was measured at 450 nm in the Halo Led 96. Cell mortality was assessed according to plasma membrane integrity; for that, the Cell-Tox Green Cytotoxicity Assay (Promega) was used. To this end, the protocol recommended by the manufacturer was followed: the dye was prepared at a concentration of 1:500 in the given buffer and 100 µL were directly added to the wells to a final concentration of 1:1000. After 15 min of incubation at 37°C and protected from light, the fluorescence was measured in the Promega GloMax Discover at a wavelength of 492 nm excitation and 535 nm emission.

Long-term observation was performed at 24 h, 72 h, and 7 days after the placement of the scaffold through the Live/Dead Cell Viability Assay (Thermo Fisher) in order to monitor directly the cell status and phenotype. For that purpose, calcein AM and ethidium homodimer-1 were added to a final concentration of 1:2000 and 1:1000, respectively, from which 200 µL of the preparation were added to the 24 wells. After 15 min of incubation, images were taken with the ZEISS LSM 900 confocal microscope.

In addition to the study conditions, positive (CTR+) and negative (CTR-) controls were included. For CTR+, cells seeded in the same conditions, but without biomaterial, were used, while cells were treated with lysis solutions to provoke cell death for CTR-. In the case of the Cell-Tox Green Cytotoxicity Assay, the given buffer was employed and, in the case of CCK-8 and Live/Dead Cell Viability Assay, dimethyl sulfoxide (DMSO) (Sigma) was used instead. Each condition was analyzed in fourfold.

For short-term biocompatibility, results were relativized to the controls. In the case of mortality, CTR- was considered having 100% of mortality and CTR+ having 0%; they were considered inversely in the assay of metabolic activity.

3. Results and discussion

3.1. Chitin extraction yield and characterization

Since insects have a large protein content, deproteinization must be carried out and the temperature, NaOH concentration, and reaction time used in this process influence the extraction yield[32]. In this work, the extraction yield achieved was 25.52%. Other Diptera species, such as *Hermetia illucens*, have also shown values around 20%–25%[33]. Considering that the extraction yield of chitin from insects is similar to that obtained from crustacean shell waste, insects can be considered an alternative chitin source[34].

Chitin presents in three crystalline forms, known as α, β, and γ, with α-chitin being the most abundant form[35,36]. The α- and β-forms can be differentiated by FTIR analysis. The spectrum of the α-form has two bands at 1650 and 1620 cm^{-1}[37], while the β-form has only one band at 1630 cm^{-1}[38]. As can be seen in Figure 1A, the amide I band was divided into two peaks, which appear at about 1650 (shoulder) and 1622 cm^{-1}; therefore, α-chitin was obtained in this work. α-chitin is usually found in the cuticles of insects[39]. Other characteristic bands of chitin are amide II (1550 cm^{-1}) and amide III (1309 cm^{-1})[40]. Moreover, a major peak around 3425 cm^{-1} is due to O-H and two sharper peaks at 3255 and 3107 cm^{-1} are attributed to N-H[41,42]. The peak around 1010 cm^{-1} is associated to C-O stretching. These characteristic bands indicate the high purity of chitin isolated from fruit fly pupae[40].

In order to analyze thermal events occurred in chitin extracted from fruit fly pupae, DSC analysis was performed and results are shown in Figure 1B. As can be observed, chitin showed an endothermic peak around 75°C, ascribed to the evaporation of entrapped water[43].

Additionally, derivative thermo-gravimetry (DTG) was carried out and curves are shown in Figure 1C. The first mass loss step was found around 57°C, related to the evaporation of water. The second mass loss step was observed around 385°C, attributed to the decomposition of the polysaccharide structure[44]. It is worth highlighting that chitin was degraded before reaching the fusion temperature, a typical behavior of polysaccharides[45].

As mentioned in the above, there are three crystalline forms of chitin, known as α, β, and γ, with α-chitin being the most abundant and stable form. These chitin forms have different chain arrangements in the crystalline region and, in particular, the α-form has an antiparallel arrangement[46]. As can be seen in XRD patterns (Figure 1D), chitin showed a high level of crystallinity, with XRD peaks observed at 9°, 19°, 21°, and 23°, characteristic of α-chitin[27]. Sharp peaks around 9° and 19° are (0 2 0) and (1 1 0) diffraction planes of the orthorhombic crystal structure[6]. Additionally, a number of XRD peaks are attributed to some impurities found in chitin from insects, as also shown by other authors[34]. These results are similar to those reported for chitin extracted from other insects[39]. Regarding crystallinity, the CrI value found was 86%, in accordance with literature[34]. It should be noted that the nature of the organism from which the chitin is extracted and the conditions used in the process can affect the crystallinity values[47].

^{13}C NMR analysis was performed to confirm that chitin powder extracted from fruit fly pupae showed the typical α-chitin ^{13}C NMR spectrum. As shown in Figure 1E, ^{13}C NMR spectrum contains eight well-defined peaks ranging from 20 to 190 ppm, corresponding to C1-C6, CH_3 and C=O carbons. Specifically, the signals associated to C1-C6 were clustered in the 50–110 ppm region: C1 (103.73ppm), C2 (54.80 ppm), C3 (73.11 ppm), C4 (83.08 ppm), C5 (75.24 ppm), and C6 (60.62 ppm). Meanwhile, methyl and carbonyl carbons showed peaks at 23 ppm and 173 ppm, respectively[48].

Additionally, elemental analysis was performed to calculate the DA of chitin. The nitrogen content of chitin found was 4.5%, a significant indicator of its purity[49]. In chitin samples with high percentages of nitrogen, protein residues can be present[50]. The DA value for chitin was calculated as 99%, so it can be concluded that the extraction process allowed obtaining chitin with high purity.

3.2. Rheological properties of 3DP and ES inks

First of all, rheological analysis was carried out to determine the temperature range for 3D printing. As can be observed in Figure 2A and C, viscosity values decreased when shear rate increased, indicating that 3DP and ES inks showed shear thinning behavior, a favorable performance for both 3D printing and electrospinning techniques. Regarding G' and G'' moduli (Figure 2B and D), these values did not change a lot at different frequencies for 3DP inks, while they showed a noticeable increase for ES inks at high frequencies. 3DP inks showed higher storage modulus (G') than loss modulus (G'') and, thus, tan $\delta < 1$, while ES inks showed the opposite tendency during the entire frequency sweep. Therefore, it can be said that 3DP inks had solid-like behavior, while ES inks had liquid-like behavior[51,52]. The two moduli joined at high frequency values for both inks.

Regarding the effect of temperature on viscosity (Table 2), zero shear viscosity values were reduced by half

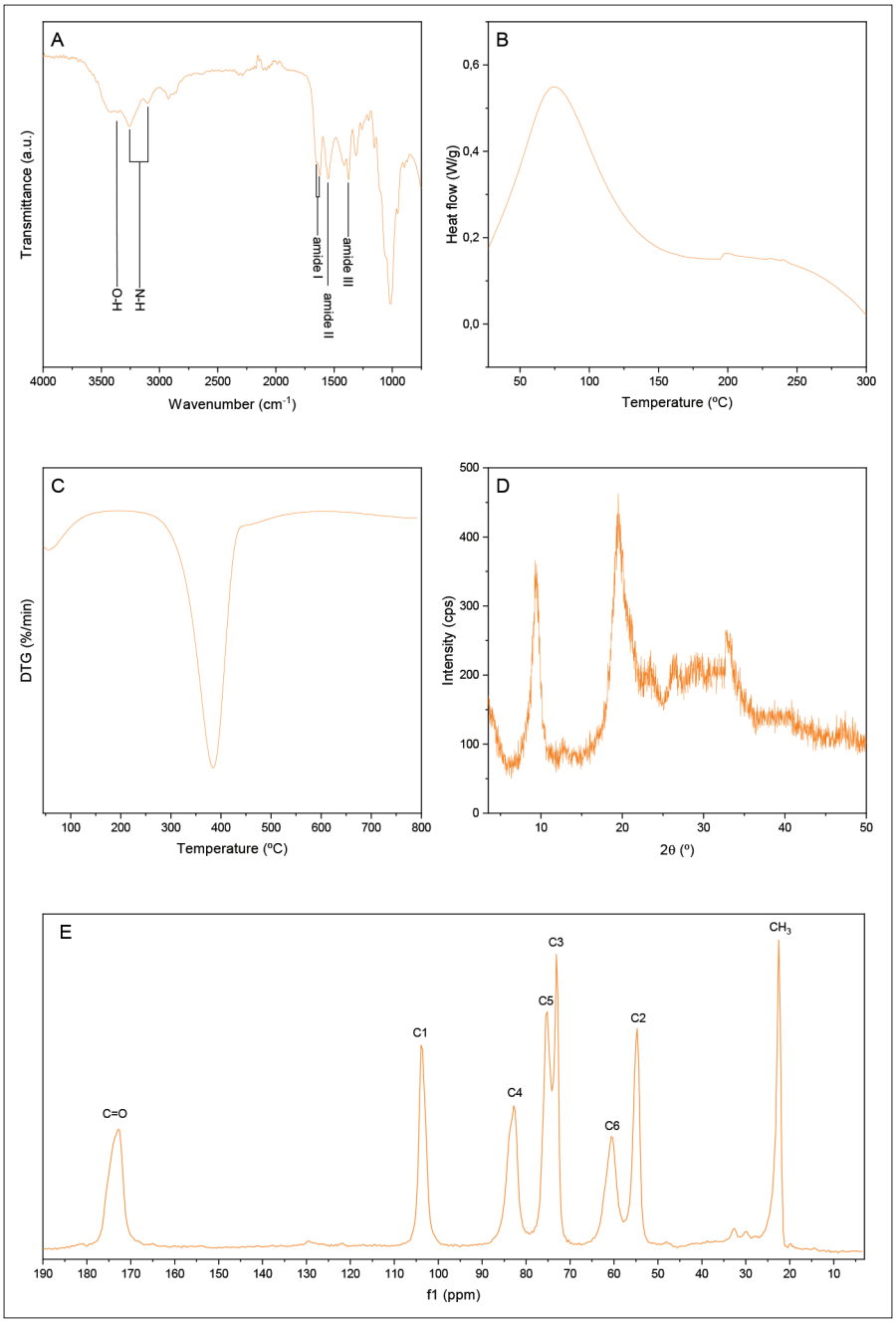

Figure 1. Physicochemical characterization of chitin powder extracted from fruit fly pupae. (A) FTIR spectra, (B) DSC thermogram, (C) DTG curves, (D) XRD patterns, and (E) ^{13}C NMR spectrum.

from 30°C to 35°C for 3DP inks. For ES samples, zero shear viscosity value was very low, suggesting that the material will not present difficulties to be extruded and thus will not require purge-type printing strategies. Additionally, m parameter was also the lowest at 35°C, indicating that the samples at this temperature are the least viscous at high shear values. This effect is favorable for 3D printing, because low viscosities are required to facilitate material extrusion through the nozzle (high shear values)[51]. However, in addition to rheological properties, other factors must be considered in order to select the most appropriate temperature for 3D printing. In this work, since chitin sedimentation on the tip can cause nozzle clogging, a lower temperature was required to ensure a homogenous chitin dispersion in the extruded 3DP ink. As a consequence, temperature values selected to process

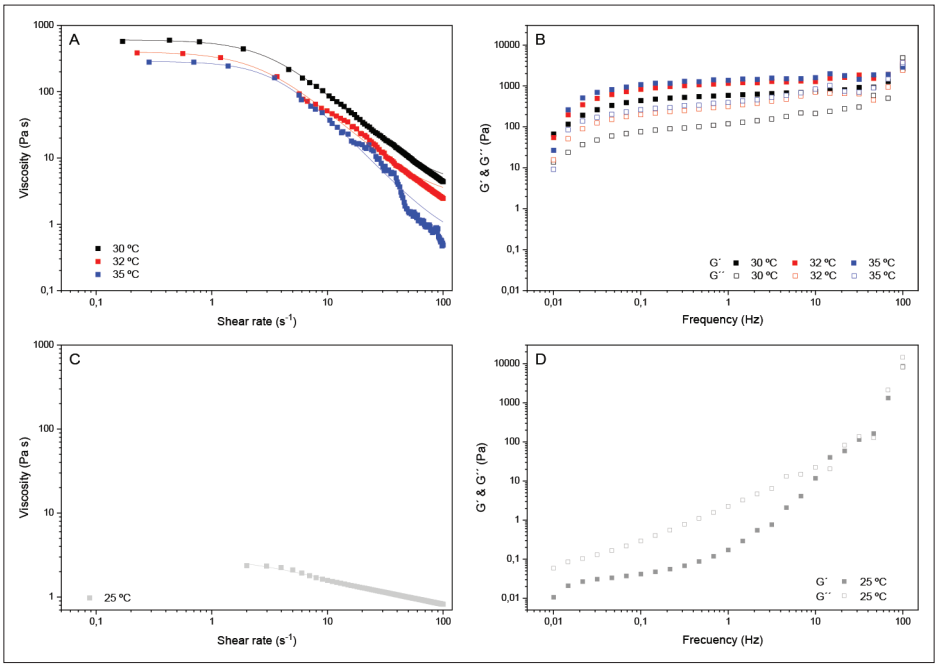

Figure 2. (A) Shear sweep and (B) frequency sweep tests for 3DP inks at 30°C, 32°C, and 35°C. (C) Shear sweep and (D) frequency sweep tests for ES inks at 25°C.

Table 2. Zero shear rate viscosity (μ_0), infinite shear viscosity ($\mu\infty$), time constant (C), and rate constant (m) of Cross model for 3DP and ES samples

Sample	T (°C)	μ_0 (Pa s)	$\mu\infty$ (Pa s)	C (s)	m	R^2
3DP	30	605.77	3.59	0.30	1.66	0.99
	32	400.25	2.29	0.34	1.61	0.99
	35	287.65	0.45	0.27	0.86	0.99
ES	25	3.29	0.61	0.18	0.82	0.99

the scaffold were 25°C and 32°C for ES and 3DP inks, respectively.

3.3. Mucoadhesion and textural properties of 3DP inks

Mucoadhesion is defined as a state in which two materials (mucin and natural or synthetic polymer) adhere to each other via interfacial forces for a certain period of time[53,54]. Mucoadhesive polymers interact with mucosal membranes because of their hydrophilicity and through different functional organic groups. These interactions might be covalent or non-covalent[53,55]. In this work, mucoadhesion tests were performed to assess the adhesion behavior of 3DP inks. As shown in Figure 3, the value of the maximum force to separate the 3DP ink from mucin was 7.47 N, and the adhesion work, calculated by integrating the area under the curve, was 6.96 mJ, which was higher than those found in the literature for mucoadhesive gelatin-based materials[56]. Mucin, a negatively charged highly glycosylated protein, can provide physical interactions (hydrogen bonds or electrostatic forces) with other polymers[55]. Therefore, in contact with the gelatin present in 3DP ink, noncovalent interactions can be formed through –COOH, $–NH_2$, and –OH polar groups present in both proteins[53]. As a result, good mucoadhesion performance was observed for 3DP inks. This behavior is considered interesting for biomedical applications in order to address the necessity to stick to target surfaces and induce cell proliferation[17].

TPA was carried out to assess the mechanical properties of the scaffold under compression forces. TPA is commonly used to study food-related materials[57], although it is a good approximation to analyze other types of applications like hydrogels for scaffolds in biomedical applications[58,59]. TPA consists of two compression cycles with a recovery time between them, and it is typically represented as a curve of force vs time[60], as shown in Figure 4 for 3DP inks. Two peaks were observed on the positive side (marked as 2 and 5) and a third peak on the negative side, whose area (marked in green) represents adhesiveness (1.27 ± 0.43 g·s). The first peak describes the required force for a given deformation and represents the material hardness (25.21 ± 7.54 g). The ratio of the positive force area during the second compression to that during the first compression (marked in red) is related to the cohesiveness (1.02 ± 0.04). This parameter is related to the deformation degree of the

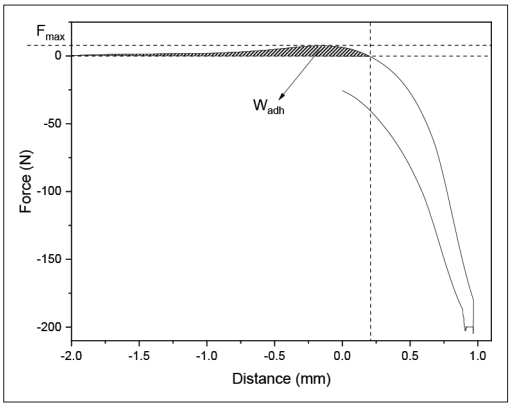

Figure 3. Load-deformation curves for 3DP inks.

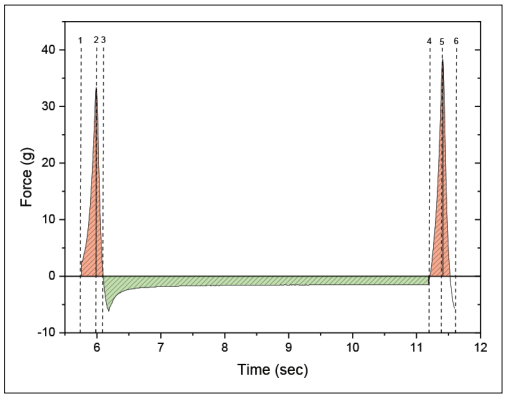

Figure 4. Textural profile analysis (TPA) of 3DP inks.

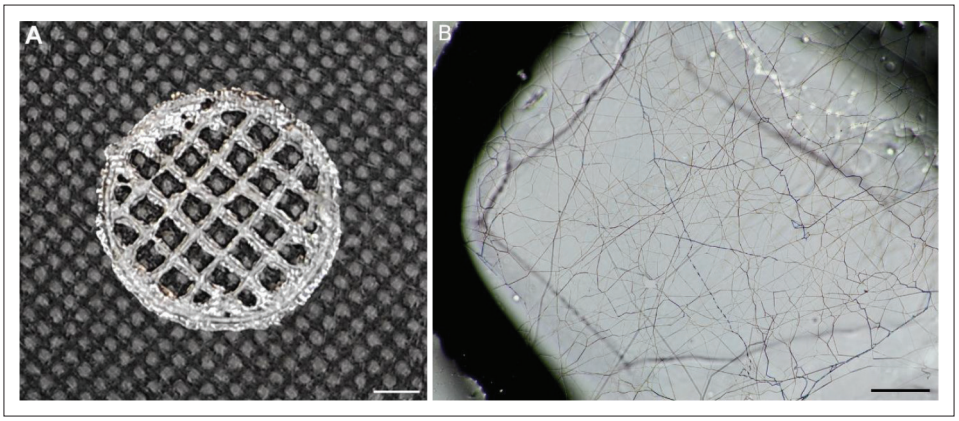

Figure 5. Optical images of (A) the hybrid scaffold macrostructure (scale bar = 4 mm) and (B) the nanofibrous mat on the pore of the 3D-printed scaffold (scale bar = 200 μm).

material before breaking and it indicates the strength of the internal bonds of the material[59]. Since cohesiveness is the ratio between the areas of the second and the first cycles, the value close to 1 suggested that the material recovered the shape.

3.4. Characterization of 3DP-ES scaffolds

The shape fidelity and dimensional stability of the scaffold is shown in Figure 5A, where an image of a 3DP-ES scaffold, obtained by optical microscopy, can be seen. Additionally, the electrospun mat attached to the 3D-printed layer can be observed in Figure 5B. The resulting scaffolds showed an average porosity of 2.5 mm in the 3D-printed layer and an average value of 64 μm in the electrospun layer. This porosity can allow the cells to seed without falling to the bottom of the culture plate so as to ensure 3D spatial deposition[15,22]. Since the combination of electrospun nanofibers with larger structures resulted in complex hierarchical scaffolds that can mimic the highly organized structure of tissues and improve biological performance, biocompatibility tests were carried out. Results showed that this structure ensures the desired interconnected porous architecture to achieve successful growth of cell culture.

With the aim of assessing the potential of these multilayered scaffolds for tissue regeneration, such as wound healing, biocompatibility was determined using human dermal fibroblasts. The short-term biocompatibility (Figure 6) was evaluated based on the metabolic activity and cell mortality along 72 h. Regarding the activity, cells had optimal activity values from the first date (75.0%), showing an ascending trend with the course of the days (91.8% at 48 h and 106.8% at 72 h). Additionally, the cell mortality was maintained around 10% along the studied time points (10.3, 7.6, and 8.4% at 24, 48 and 72 h, respectively).

Concerning long-term biocompatibility assay, the cells observed with the live/dead fluorescence kit showed optimal results (Figure 7). From 1 to 7 days of culture, the vast majority of the cells were alive, although some mortality labeling was observed. This tendency, although non-significant, could have been due to the high confluence of the culture. Likewise, the cells showed a normal fibroblastic phenotype, with spindle-shaped, central and elliptical nucleus and long cytoplasmic prolongations.

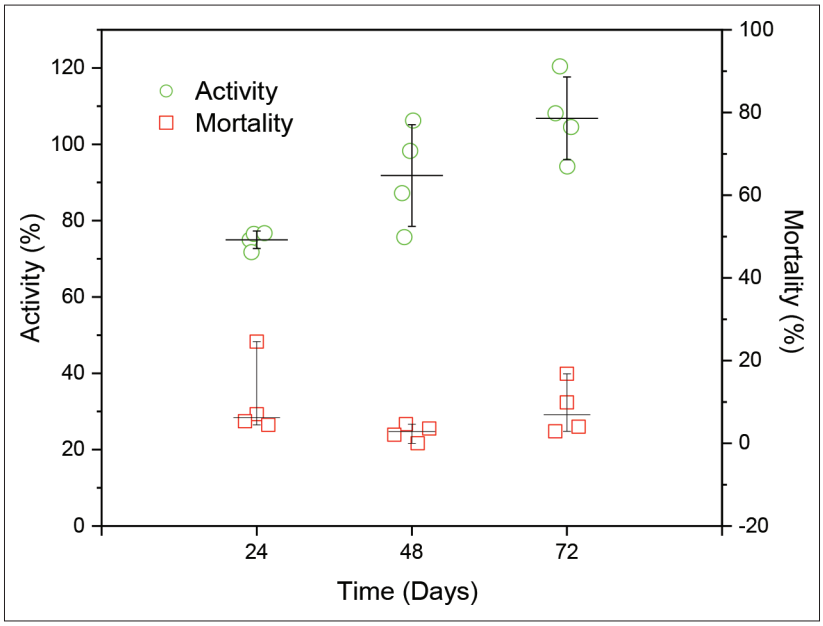

Figure 6. Biocompatibility assessment through the exposition of the scaffold to HS27 cells at 24, 48 and 72 h of culture.

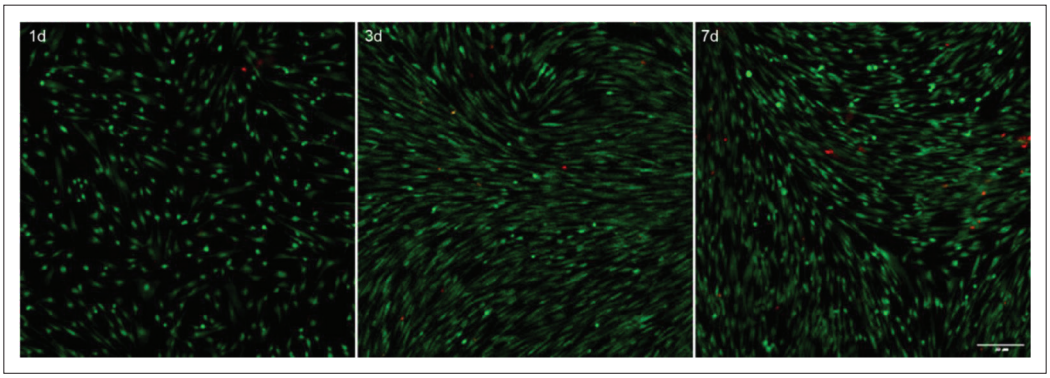

Figure 7. Images taken following the live/dead cell viability assay at 1, 3, and 7 days of culture after the direct exposure of the scaffolds. Live and dead cells are shown in green and red, respectively. Scale bar represents 50 μm.

4. Conclusion

Fly fruit pupae were found to be good candidates for chitin extraction, as proven by the high extraction yield obtained. Additionally, the purity of the chitin obtained was high, as suggested by FTIR and XRD analyses. This chitin was used to prepare gelatin-based inks for 3DP, while ES inks were prepared with gelatin and PVA. Both inks had shear thinning behavior, required for additive manufacturing processes, as shown by the rheological assessment. Furthermore, 3DP inks exhibited good mucoadhesion and textural properties for tissue engineering applications. It is worth noting the good replicability of the scaffolds manufactured by combining 3DP and ES. Resulting scaffolds showed an interconnected pore architecture, favorable for cellular adhesion and growth. Therefore, cell viability was tested and biocompatibility was confirmed.

Acknowledgments

None.

Funding

This work was supported by the Basque Government through the research groups of the Basque university system (IT1658-22) and through Elkartek Program (KK-2022/00019). Work at Biodonostia was supported by Project PI19/01621, funded by Instituto de Salud Carlos III (ISCIII) and co-funded by the European Union. J.U. thanks the University of the Basque Country (ESPDOC21/74).

T.C. (PRE_2021_1_0254) and A.I. (PRE_2019_1_0031) thank the Basque Government for their fellowships.

Conflict of interest

The authors declare they have no competing interests.

Author contributions

Conceptualization: Teresa Carranza, Pedro Guerrero
Formal analysis: Teresa Carranza, Jone Uranga, Ainhoa Irastorza
Funding acquisition: Ander Izeta, Koro de la Caba
Investigation: Teresa Carranza, Jone Uranga, Ainhoa Irastorza
Methodology: Pedro Guerrero
Project administration: Ander Izeta, Koro de la Caba
Resources: Ander Izeta, Koro de la Caba
Supervision: Ander Izeta, Koro de la Caba, Pedro Guerrero
Writing – original draft: Teresa Carranza, Jone Uranga, Ainhoa Irastorza
Writing – review & editing: Ander Izeta, Koro de la Caba, Pedro Guerrero

Ethics approval and consent to participate

Not applicable.

Consent for publication

Not applicable.

Availability of data

Not applicable.

References

1. Omran BA, Baek K-H, 2022, Valorization of agro-industrial biowaste to green nanomaterials for wastewater treatment: Approaching green chemistry and circular economy principles. *J Environ Manage*, 311:114806.
2. Águila-Almanza E, Low SS, Hernández-Cocoletzi H, *et al*., 2021, Facile and green approach in managing sand crab carapace biowaste for obtention of high deacetylation percentage chitosan. *J Environ Chem Eng*, 9:105229.
3. Ren B, Weitzel KA, Duan X, *et al*., 2022, A comprehensive review on algae removal and control by coagulation-based processes: mechanism, material, and application. *Sep Purif Technol*, 293:121106.
4. Tuão Gava CA, da Silva JC, Simões WL, *et al*., 2021, Impact of soil texture on conidia movement and residual effect of entomopathogenic fungi applied through irrigation to control fruit-fly pupae in mango orchards. *Biol Control*, 163:104559.
5. Wappner P, Kramer KJ, Hopkins TL, *et al*., 1995, White pupa: a Ceratitis capitata mutant lacking catecholamines for tanning the puparium. *Insect Biochem Mol Biol*, 25:365.
6. Tsurkan MV, Voronkina A, Khrunyk Y, *et al*., 2021, Progress in chitin analytics. *Carbohydr Polym*, 252:117204.
7. Chen C, Deng S, Yang Y, *et al*., 2018, Highly transparent chitin nanofiber/gelatin nanocomposite with enhanced mechanical properties. *Cellulose*, 25:5063.
8. Zheng Y, Li X, Huang Y, *et al*., 2022, Two colorimetric films based on chitin whiskers and sodium alginate/gelatin incorporated with anthocyanins for monitoring food freshness. *Food Hydrocolloid*, 127:107517.
9. Orooji Y, Han N, Nezafat Z, *et al*., 2022, Valorisation of nuts biowaste: Prospects in sustainable bio(nano)catalysts and environmental applications. *J Clean Prod*, 347:131220.
10. Álvarez-Castillo E, Felix M, Bengoechea C, *et al*., 2021, Proteins from Agri-Food industrial biowastes or co-products and Their applications as green materials. *Foods*, 10:981.
11. Rodriguez Colon R, Nayak VV, Parente PEL, *et al*., 2022, The presence of 3D printing in orthopedics: A clinical and material review. *J Orthop Res*, 40:1–13.

    https://doi.org/10.1002/jor.25388
12. Smith ML, Jones JFX, 2018, Dual-extrusion 3D printing of anatomical models for education. *Anat Sci Educ*, 11:65.
13. Dey D, Srinivas D, Panda B, *et al*., 2022, Use of industrial waste materials for 3D printing of sustainable concrete: A review. *J Clean Prod*, 340:130749.
14. Mustapha KB, Metwalli KM, 2021, A review of fused deposition modelling for 3D printing of smart polymeric materials and composites. *Eur Polym J*, 156:110591.
15. Dong Q, Zhang M, Zhou X, *et al*., 2021, 3D-printed Mg-incorporated PCL-based scaffolds: A promising approach for bone healing. *Mater Sci Eng C*, 129:112372.
16. Xie Z, Gao M, Lobo AO, *et al*., 2020, 3D bioprinting in tissue engineering for medical applications: The classic and the hybrid. *Polymers*, 12:1717.

    https://doi.org/10.3390/polym12081717
17. Nam S, Mooney D, 2021, Polymeric Tissue Adhesives. *Chem Rev*, 121:11336.
18. Afewerki S, Sheikhi A, Kannan S, *et al*., 2019, Gelatin-polysaccharide composite scaffolds for 3D cell culture and tissue engineering: Towards natural therapeutics. *Bioeng Transl Med*, 4:96.
19. Nhu CN, Thi NV, Hoang NN, *et al*., 2021, Characterization of gelatin and PVA nanofibers fabricated using electrospinning process. in Advances in Engineering Research and application, Sattler KU, Nguyen DC, Vu NP, Long BT, Puta H (Eds.), Springer International Publishing, Cham, 216–222.

20. Li T, Sun M, Wu S, 2022, State-of-the-Art review of electrospun gelatin-based nanofiber dressings for wound healing applications. *Nanomaterials*, 12:784.

21. Thangprasert A, Tansakul C, Thuaksubun N, *et al*., 2019, Mimicked hybrid hydrogel based on gelatin/PVA for tissue engineering in subchondral bone interface for osteoarthritis surgery. *Mater Design*, 183:108113.

22. Abel SB, Ballarin FM, Abraham GA, 2020, Combination of electrospinning with other techniques for the fabrication of 3D polymeric and composite nanofibrous scaffolds with improved cellular interactions. *Nanotechnology*, 31:172002.

23. Bidgoli MR, Alemzadeh I, Tamjid E, *et al*., 2019, Fabrication of hierarchically porous silk fibroin-bioactive glass composite scaffold via indirect 3D printing: Effect of particle size on physico-mechanical properties and in vitro cellular behavior. *Mater Sci Eng C*, 103:109688.

24. Hernandez JL, Woodrow KA, 2022, Medical applications of porous biomaterials: Features of porosity and tissue-specific implications for biocompatibility. *Adv Healthc Mater*, 11:2102087.

25. Ma P, Wu W, Wei Y, *et al*., 2021, Biomimetic gelatin/chitosan/polyvinyl alcohol/nano-hydroxyapatite scaffolds for bone tissue engineering. *Mater Design*, 207:109865.

26. Sánchez-Cardona Y, Echeverri-Cuartas CE, López MEL, *et al*., 2021, Chitosan/Gelatin/PVA scaffolds for beta pancreatic cell culture. *Polymers*, 13:2372.

27. Chen Y-M, Pekdemir S, Bilican I, *et al*., 2021, Production of natural chitin film from pupal shell of moth: Fabrication of plasmonic surfaces for SERS-based sensing applications. *Carbohydr Polym*, 262:117909.

28. Kucukgulmez A, Celik M, Yanar Y, *et al*., 2011, Physicochemical characterization of chitosan extracted from metapenaeus stebbingi shells. *Food Chem*, 126:1144.

29. Pössl A, Hartzke D, Schmidts TM, *et al*., 2021, A targeted rheological bioink development guideline and its systematic correlation with printing behavior. *Biofabrication*, 13:035021.

30. Schneider CA, Rasband WS, Eliceiri KW, 2012, NIH Image to ImageJ: 25 years of image análisis. *Nat Methods*, 9:671.

31. International Organization for Standardization, 2009, Biological evaluation of medical devices - Part 5: Tests for in vitro cytotoxicity. ISO 10993-5:2009, https://www.iso.org/cms/render/live/en/sites/isoorg/contents/data/standard/03/64/36406.html

32. Liao J, Huang H, 2020, Extraction of a novel fungal chitin from hericium erinaceus residue using multistep mild procedures. *Int J Biol Macromol*, 156:1279.

33. Antonov A, Ivanov G, Pastukhova N, *et al*., 2019, Production of chitin from dead hermetia illucens. *IOP Conf Ser Earth Environ Sci*, 315:042003.

34. Mohan K, Ganesan AR, Muralisankar T, *et al*., 2020, Recent insights into the extraction, characterization, and bioactivities of chitin and chitosan from insects. *Trends Food Sci Technol*, 105:17.

35. Joseph SM, Krishnamoorthy S, Paranthaman R, *et al*., 2021, A review on source-specific chemistry, functionality, and applications of chitin and chitosan. *Carbohydr Polym Technol Appl*, 2:100036.

36. Wei A, Fu J, Guo F, 2021, Mechanical properties of chitin polymorphs: A computational study. *J Mater Sci*, 56:12048.

37. Złotko K, Waśko A, Kamiński DM, *et al*., 2021, Isolation of Chitin from Black Soldier Fly (Hermetia illucens) and Its usage to metal sorption. *Polymers*, 13:818.

38. Uranga J, Etxabide A, Cabezudo S, *et al*., 2020, Valorization of marine-derived biowaste to develop chitin/fish gelatin products as bioactive carriers and moisture scavengers. *Sci Total Environ*, 706:135747.

39. Jantzen da Silva Lucas A, Quadro Oreste E, Leão Gouveia Costa H, *et al*., 2021, Extraction, physicochemical characterization, and morphological properties of chitin and chitosan from cuticles of edible insects. *Food Chem*, 343:128550.

40. Kaya M, Sofi K, Sargin I, *et al*., 2016, Changes in physicochemical properties of chitin at developmental stages (larvae, pupa and adult) of Vespa crabro (wasp). *Carbohydr Polym*, 145:64.

41. Dhanabalan V, Xavier KAM, Eppen S, *et al*., 2021, Characterization of chitin extracted from enzymatically deproteinized acetes shell residue with varying degree of hydrolysis. *Carbohydr Polym*, 253:117203.

42. Soetemans L, Uyttebroek M, Bastiaens L, 2020, Characteristics of chitin extracted from black soldier fly in different life stages. *Int J Biol Macromol*, 165:3206.

43. Wardhono EY, Pinem MP, Kustiningsih I, *et al*., 2021, Heterogeneous deacetylation reaction of chitin under low-frequency ultrasonic irradiation. *Carbohydr Polym*, 267:118180.

44. Ilyas HN, Zia KM, Rehman S, *et al*., 2021, Utilization of shellfish industrial waste for isolation, purification, and characterizations of Chitin from Crustacean's sources in Pakistan. *J Polym Environ*, 29:2337.

45. Agulló E, Mato R, Peniche C, *et al*., 2004, Quitina y quitosano: obtención, caracterización y aplicaciones, Pastor de Abram A (Eds.), Pontifica universidad católica del peru, fondo editorial, 105-154.

46. Sabab A, Liu S, Javadiyan S, *et al*., 2021, The effect of chemical and structural modifiers on the haemostatic process and cytotoxicity of the beta-chitin patch. *Sci Rep*, 11:18577.

47. Aranaz I, Mengíbar M, Harris R, *et al*., 2009, Functional characterization of chitin and chitosan. *Curr Chem Biol*, 3:203.

48. Fernández-Marín R, Hernández-Ramos F, Salaberria AM, *et al*., 2021, Eco-friendly isolation and characterization of nanochitin from different origins by microwave irradiation: Optimization using response surface methodology. *Int J Biol Macromol*, 186:218.

49. Tan YN, Chin YL, Chen WN, 2021, Comparison of sustainable lipid and protein removal methods for the isolation of insect chitin from Black Soldier Fly exoskeleton. *ACS Food Sci Technol*, 1:698.

50. Ssekatawa K, Byarugaba DK, Wampande EM, *et al*., 2021, Isolation and characterization of chitosan from ugandan edible mushrooms, Nile perch scales and banana weevils for biomedical applications. *Sci Rep*, 11:4116.

51. Lee SC, Gillispie G, Prim P, *et al*., 2020, Physical and chemical factors influencing the printability of hydrogel-based extrusion bioinks. *Chem Rev*, 120:10834.

52. Tian S, Zhao H, Lewinski N, 2021, Key parameters and applications of extrusion-based bioprinting. *Bioprinting*, 23:e00156.

53. Ahmady A, Abu Samah NH, 2021, A review: Gelatine as a bioadhesive material for medical and pharmaceutical applications. *Int J Pharm*, 608:121037.

54. Spence Leung SH, Robinson JR, 1987, The contribution of anionic polymer structural features to mucoadhesion. *J Control Release*, 5:223.

55. Bassi da Silva J, de S. Ferreira SB, Reis AV, *et al*., 2018, Assessing mucoadhesion in polymer gels: The effect of method type and instrument variables. *Polymers*, 10:254.

56. Jovanović M, Tomić N, Cvijić S, *et al*., 2021, Mucoadhesive gelatin buccal films with propranolol hydrochloride: Evaluation of mechanical. *Pharmaceutics*, 13:273.

57. Sakaguchi K, Tobe Y, Yang J, *et al*., 2021, Bioengineering of a scaffold-less three-dimensional tissue using net mould, Biofabrication. *Biofabrication*, 13:045019.

58. Kuo C-C, Qin H, Cheng Y, *et al*., 2021, An integrated manufacturing strategy to fabricate delivery system using gelatin/alginate hybrid hydrogels: 3D printing and freeze-drying. *Food Hydrocolloid*, 111:106262.

59. Zhang C, Wang C-S, Therriault D, *et al*., 2022, Development of aqueous protein/polysaccharide mixture-based inks for 3D printing towards food applications. *Food Hydrocolloid*, 107742.

60. Breene WM, 1975, Application of texture profile analysis to instrumental food texture evaluation. *J Texture Stud*, 6:53.